Electronic Supplementary Information for Soft Matter

Nano-to-meso structure of cellulose nanocrystals phases in ethylene-glycol-water mixtures

David Attia[1], Neta Cohen[1], Guy Ochbaum[1], Yael Levi-Kalisman[2], Ronit Bitton[1,3], Rachel Yerushalmi – Rozen[1,3]*

1. Department of Chemical Engineering, Ben-Gurion University of the Negev, 84105 Beer-Sheva, Israel.
2. The Center for Nanoscience and Nanotechnology, and The Institute of Life Sciences, the Hebrew University of Jerusalem, Israel
3. The Ilse Katz Institute for Nanoscience and Technology, Ben-Gurion University of the Negev, 84105 Beer-Sheva, Israel.

Corresponding author: rachely@bgu.ac.il

S.1 SLO model

The emergence of alignment in idealized monodispersed (non-charged) rods interacting via a mean field excluded-volume potential in athermal solvent was derived by Onsager[1] and Flory.[2,3] The model describes the competition between the contribution of orientational entropy and the excluded-volume to the free energy. Flory's lattice-based theory accounts for excluded-volume interactions and allows for attractive solvent-mediated inter-particle interactions. Both theories describe a transition from randomly oriented phase to orientationally ordered LC phase, via a biphasic region where the two coexist.

In the case of charged rods electrostatic effects are expected to shift the free energy balance but preserve the general picture. The model suggested by Stroobants, Lekkerkerker and Odijk (SLO)[4,5] modifies Onsager's theory for the phase separation of rod-like polyelectrolytes. In the framework of this model, the *effective* diameter D_{eff} of charged rods should depend on the Debye length κ^{-1} as:

$$D_{eff} = D + 5.54 \cdot \kappa^{-1} \qquad (S1)$$

For aqueous suspensions of CNCs $\kappa^{-1} = 4.25$ nm. As the Debye screening length, κ^{-1}, decreases with the relative dielectric constant $\left(\kappa^{-1} \propto \sqrt{\varepsilon_r}\right)$ a reduction in the effective diameter of each rod

is expected in EG. The dielectric constant of EG at 20 ℃ is 41.4, while that of water is 80. Thus, κ^{-1} (EG) would be $4.25/\sqrt{2}$ nm, which is about 3 nm. Following equations S1, D_{eff} of 10 nm wide CNC rod would be 33.5 nm in water and 26.6 nm in EG, leading to a higher (effective) aspect ratio (D_{eff}/L) going from water to EG. According to the SLO model,[4] the effective aspect ratio of charged rods should increase with the decrease in the relative dielectric constant.

S.2 Materials: Water content of EG, and Zeta potential the measured electrophoretic mobility in EG:Water mixtures.

The zeta potential of a colloidal particle may be calculated from the measured electrophoretic mobility via the Henry equation:

$$U_E = \frac{2\varepsilon_r \zeta}{3\eta} f(ka) \qquad (S2)$$

Where U_E is the electrophoretic mobility, ε_r is the dielectric constant, η the viscosity, ζ the zeta potential, defined as the potential at the slipping plane, and $f(ka)$ is the Henry's function. For low dielectric constant solvents and non-aqueous media, the value of $f(ka)$ is 1.0 and is referred to as Huckel approximation[6] that is applicable to elongated rods at the dilute regime.[7]

Table S1. The dielectric constant and the viscosity of solvent mixtures used in this study.

Solvent-composition	Dielectric constant ε_r	Viscosity (Pa·s, at 20 ℃) η
Native EG	41.8	0.0162
$EG_{75\%}$:$Water_{25\%}$	53.5	0.0123
$EG_{45\%}$:$Water_{55\%}$	66.7	0.0076
Water	80.4	0.0010

When the liquid media is a mixture of two solvents with different affinity for the colloidal particle, the dielectric constant and the viscosity would depend on the distance from the NP surface.

The suspensions investigated here comprise of charged cylindrical rods in a liquid mixture. For this system, the relative orientation of the rods affects the local electric field,[7] and deviation from the bulk composition of the EG:Water mixture may affect the local dielectric constant and the double-layer capacitance. We thus report the measured mobility values rather than the calculated zeta potentials.

However, if we assume that the effective surface charge of the CNCs is similar in the different suspensions, due to the presence of hydration layer (-41 mV), the following values of electrophoretic motilities are expected:

Table S2. The measured electrophoretic mobility of 0.007 vol% of CNCs suspensions in the different solvent mixtures.

Solvent-composition	Measured Mobility (μmcm/Vs)
Native EG	-0.114 ± 0.066
$EG_{75\%}$:$Water_{25\%}$	-0.375 ± 0.012
$EG_{45\%}$:$Water_{55\%}$	-0.763 ± 0.038
Water	-3.224 ± 0.184

The calculated mobility of CNCs in native EG is ~ 1/32, as compared to the mobility of CNCs in water.

The water content of as-received EG was measured by Thermogravimetric analysis (TGA), and refractive index measurements. TGA experiments were performed using a Mettler Toledo TGA/SDTA851e instrument. The measurements were carried out by heating at a constant rate of 5 ℃ min^{-1} from 40 to 500 ℃, under a constant flow of nitrogen (200 mL min^{-1}). Refractive index measurements were performed using a Rudolph J257 automatic Refractometer.

Both types of measurements indicated that the water content of non-dried EG is about 5± 0.5 vol%.

S.3 CNCs length as determined by TEM

The typical length of the CNCs rods was determined by analysis of images taken via cryo-TEM of 4.1 vol% (6 wt%) suspension in water. The average length of CNCs L = (145 ± 16) nm was determined by fitting normal distribution to the measured lengths (Figure S1).

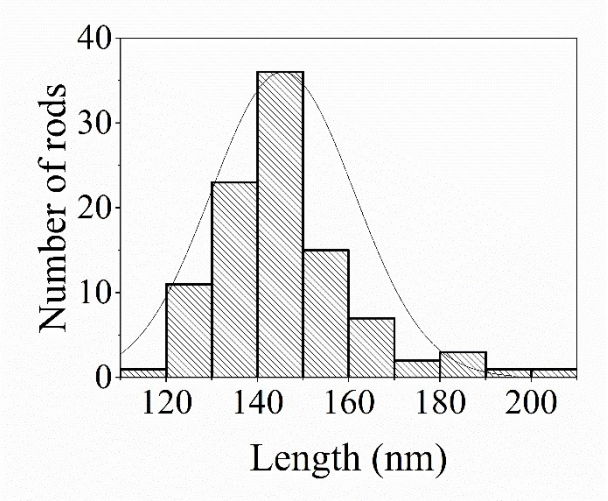

Figure S1. Distribution of CNCs length from cryo-TEM images of 4.1 vol% (6 wt%) CNCs in water.

S.4 Phase diagrams of CNCs suspensions

In Figure S2 we present phase diagrams obtained from CNCs suspensions in native EG, $EG_{45\%}$:$Water_{55\%}$, and water.

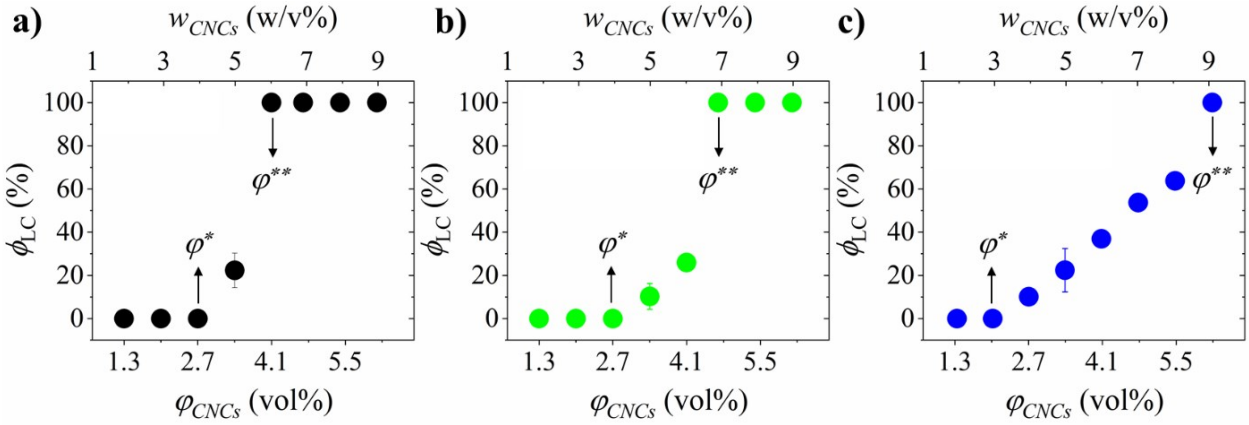

Figure S2. The phase diagrams obtained from CNCs suspensions in (a) native EG, (b) $EG_{45\%}$:$Water_{55\%}$, and (c) water.

S.5 Polarized optical microscopy (POM) measurements

In Figures S3 to S5 we present POM images of different CNCs concentrations in native EG (Figure S3), a mixture of EG and water (S4), and in water (S5). The images were taken between crossed polarizes. In liquid mixtures that contain EG, the typical fingerprint pattern of the N* is clearly observed up to a CNCs concentration where the N* is replaced by the nematic phase, probably due to kinetic arrest.

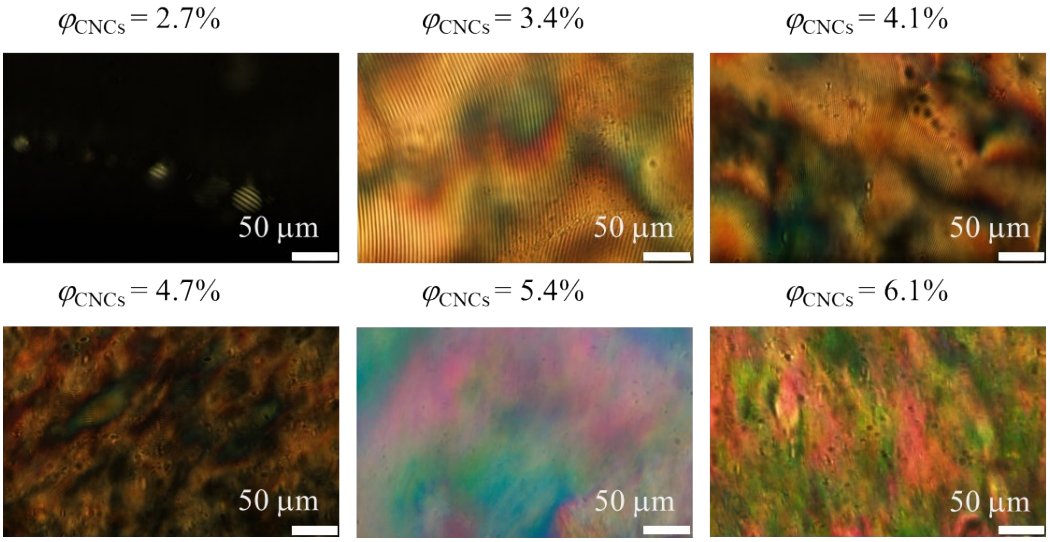

Figure S3. POM images of CNCs suspensions in native EG

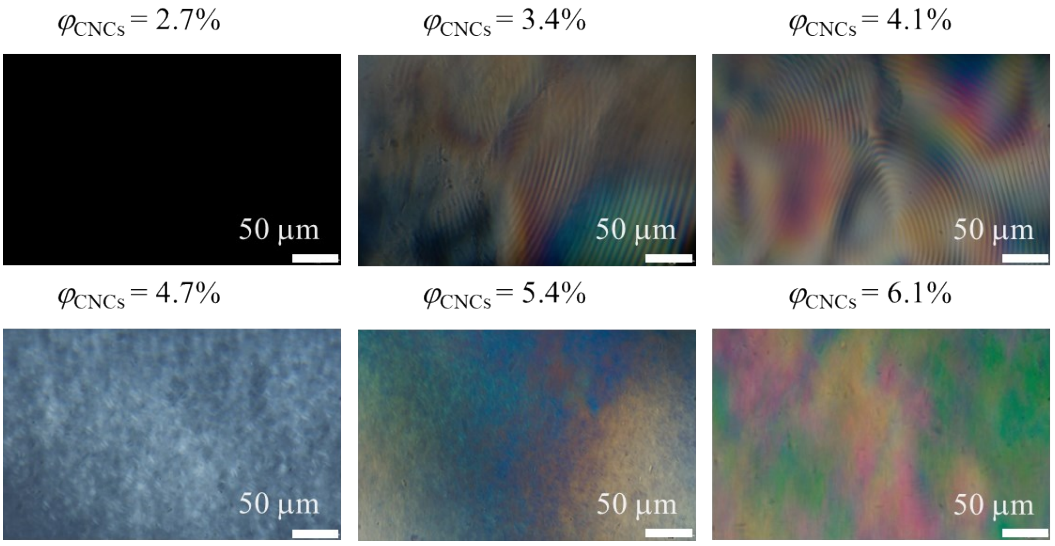

Figure S4. POM images of CNCs suspensions in $EG_{75\%}$:$Water_{25\%}$.

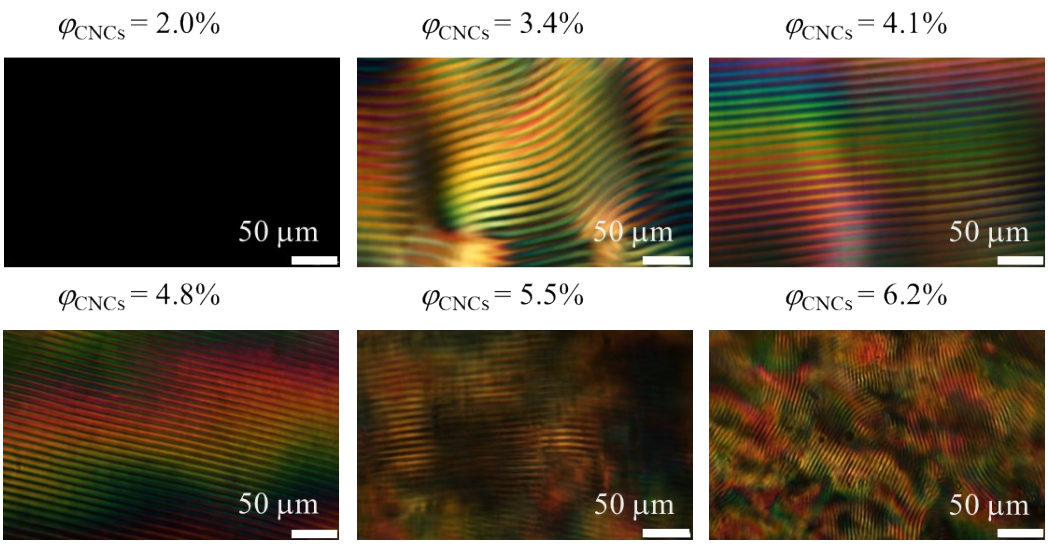

Figure S5. POM images of CNCs suspensions in water.

Table S3. Characteristic pitch values and typical diameter of the tactoids in the upper phase and LC phase of different EG:Water mixtures and CNCs volume fractions.

Solvent mixture	Volume fraction φ (vol%)	Lower phase	Upper phase Tactoids	
		Pitch (μm)	Typical diameter (μm)	Pitch (μm)
Native EG	2.7	-	22 ± 7	12 ± 1
	3.4	10 ± 2	32 ± 7	10 ± 1
	4.1	6 ± 1	-	-
	4.7	5 ± 1	-	-
$EG_{75\%}$:$Water_{25\%}$	3.4	14 ± 2	26 ± 6	17 ± 2
	4.1	12 ± 1	-	-
	4.7	9 ± 1	-	-
$EG_{45\%}$:$Water_{55\%}$	3.4	18 ± 1	16 ± 4	18 ± 2
	4.1	17 ± 1	18 ± 3	18 ± 4
	4.7	14 ± 1	-	-
	5.4	11 ± 1	-	-
	6.1	9 ± 1	-	-
Water	2.7	30 ± 2	-	-
	3.4	27 ± 1	-	-
	4.1	24 ± 1	-	-
	4.8	18 ± 2	21 ± 2	17 ± 1
	5.5	15 ± 2	37 ± 5	13 ± 1
	6.2	9 ± 1	-	-

S.6 Small-angle X-ray scattering (SAXS)

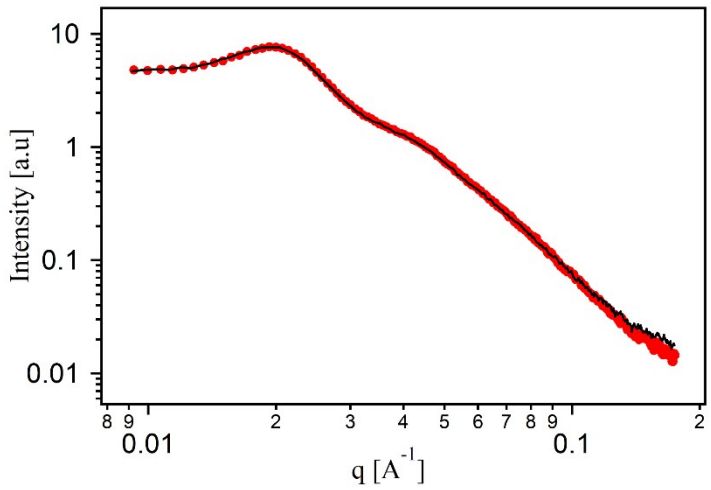

Figure S6. Fitting of the parallelepiped stacking model[8] (black line) to the SAXS pattern obtained from 4.8 vol% CNCs suspension in water.

Table S4. The width, *b,* and thickness, *a,* of CNCs particles as determined by the parallelepiped stacking model in aqueous suspensions.

CNCs volume fraction φ (vol%)	a (nm)	b (nm)
2.7	3.2	13.6
3.4	3.3	14.2
4.7	3.5	28.6
6.1	3.4	26.4

The values of q_0 and the corresponding standard deviations were estimated by fitting a standard Gaussian function to the main peaks of the Log-Log Lorentz-corrected intensities plots. Then, the average inter-particle distances and the SD (presented in Figure S7 as error bars) of the d_0 spacing were calculated.

In agreement with previous studies,[9,10] the peak position shifts to higher q values (shorter inter-particle distances) with increasing CNCs concentration (In native EG from ~ 44 nm at φ_{CNCs} =

2.0% to ~ 29 nm at φ_{CNCs} = 6.1%, and in $EG_{45\%}$:$Water_{55\%}$ from ~ 40 nm at φ_{CNCs} = 2.0% to ~ 29 nm at φ_{CNCs} = 6.1%).

Table S5. Data obtained from SAXS measurements of CNCs suspensions in native EG.

CNCs volume fraction φ (vol%)	q_0 (A^{-1})	q_1 (A^{-1})	d_0 (nm)	q_1/q_0
2.0	0.01441	0.02714	44	2
2.7	0.01547	0.02857	41	2
3.4	0.01705	0.03215	37	2
4.1	0.01805	0.03286	35	2
4.7	0.01870	0.03501	34	2
5.4	0.01984	0.03644	32	2
6.1	0.02179	0.04361	29	2

Table S6. Data obtained from SAXS measurements of CNCs suspensions in $EG_{75\%}$:$Water_{25\%}$.

CNCs volume fraction φ (vol%)	q_0 (A^{-1})	q_1 (A^{-1})	d_0 (nm)	q_1/q_0
2.0	0.01464	0.02785	43	2
2.7	0.01545	0.02714	41	2
3.4	0.01768	0.03501	36	2
4.1	0.01952	0.03573	32	2
4.7	0.01941	0.03573	32	2
5.4	0.02047	0.03859	31	2
6.1	0.02178	0.04146	29	2

Table S7. Data obtained from SAXS measurements of CNCs suspensions in $EG_{45\%}$:$Water_{55\%}$.

CNCs volume fraction φ (vol%)	q_0 (A^{-1})	q_1 (A^{-1})	d_0 (nm)	q_1/q_0
2.0	0.0156	0.03000	40	2
3.4	0.0172	0.03358	37	2
4.1	0.0180	0.03573	35	2
4.7	0.0196	0.03716	32	2
5.4	0.0209	0.04003	30	2
6.1	0.0220	0.04217	29	2

Table S8. Data obtained from SAXS measurements of CNCs suspensions in water.

CNCs volume fraction φ (vol%)	q_0 (A^{-1})	q_1 (A^{-1})	d_0 (nm)	q_1/q_0
1.3	0.01329	0.02727	47	2
2.0	0.01544	0.02857	41	2
2.7	0.01759	0.03286	36	2
3.4	0.01805	0.03358	35	2
4.1	0.01959	0.03716	32	2
4.8	0.02140	0.03931	29	2
5.5	0.02310	0.04432	27	2
6.2	0.02368	0.04719	27	2

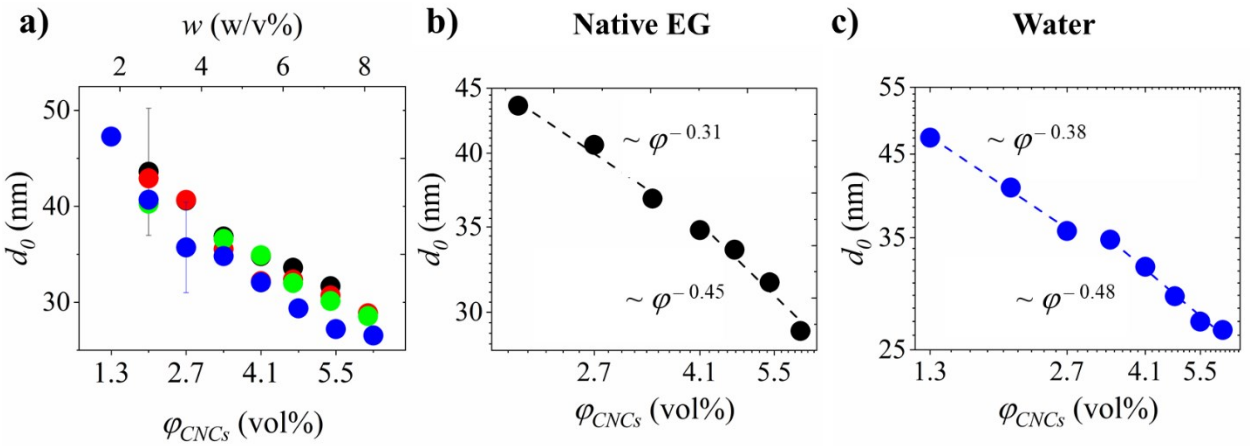

Figure S7. a) The average inter-particle distance, d_0, as a function of φ_{CNCs} in suspensions of Native EG (●), $EG_{75\%}$:$Water_{25\%}$ (●), $EG_{45\%}$:$Water_{55\%}$ (●) and water (●). The error bars are the calculated standard deviation b) Log-Log plot of d_0 as a function of CNCs concentration in Native EG and c) water.

In Figure S7 we present the average inter-particle distance, d_0, calculated from the SAXS data (Figure S7 (a)) and a fitting to a power law (Figure S7 b,c). A transition from $d_0 \sim \varphi_{CNCs}^{-0.31}$ to $d_0 \sim \varphi_{CNCs}^{-0.45}$ is observed in native EG (Figure 7 (b)). A similar trend is observed in water (Figure S7 (c)), where $d_0 \sim \varphi_{CNCs}^{-0.38}$ is transformed into $d_0 \sim \varphi_{CNCs}^{-0.48}$. While the exponents are sensitive to the exact values of the data points, the trend seems to be similar in both water and EG.

S.7 The nano and mesostructure of the isotropic phase in the bi-phasic regime

POM images of the (upper) non-birefringent phase of aqueous suspensions of CNCs suspensions show randomly oriented nematic islands (tactoids). The d_0 spacing in the SAXS curves of the upper and lower phases (φ_{CNCs} = 3.4%, 4.8% , and 5.5%, Figure S8 (d-f)) are similar, but the main peak is significantly broader in the upper phase as compared to the lower phase. The 2D scattering intensity patterns of the upper phase are isotropic and those of the lower phase are non-isotropic (similarly to the observation in EG-water mixtures). Cryo-TEM images (Figure 6 and S9) are consistent with the SAXS measurements. These observations indicate that the upper phase is comprised of randomly oriented nematic islands that do not coalesce into larger areas.

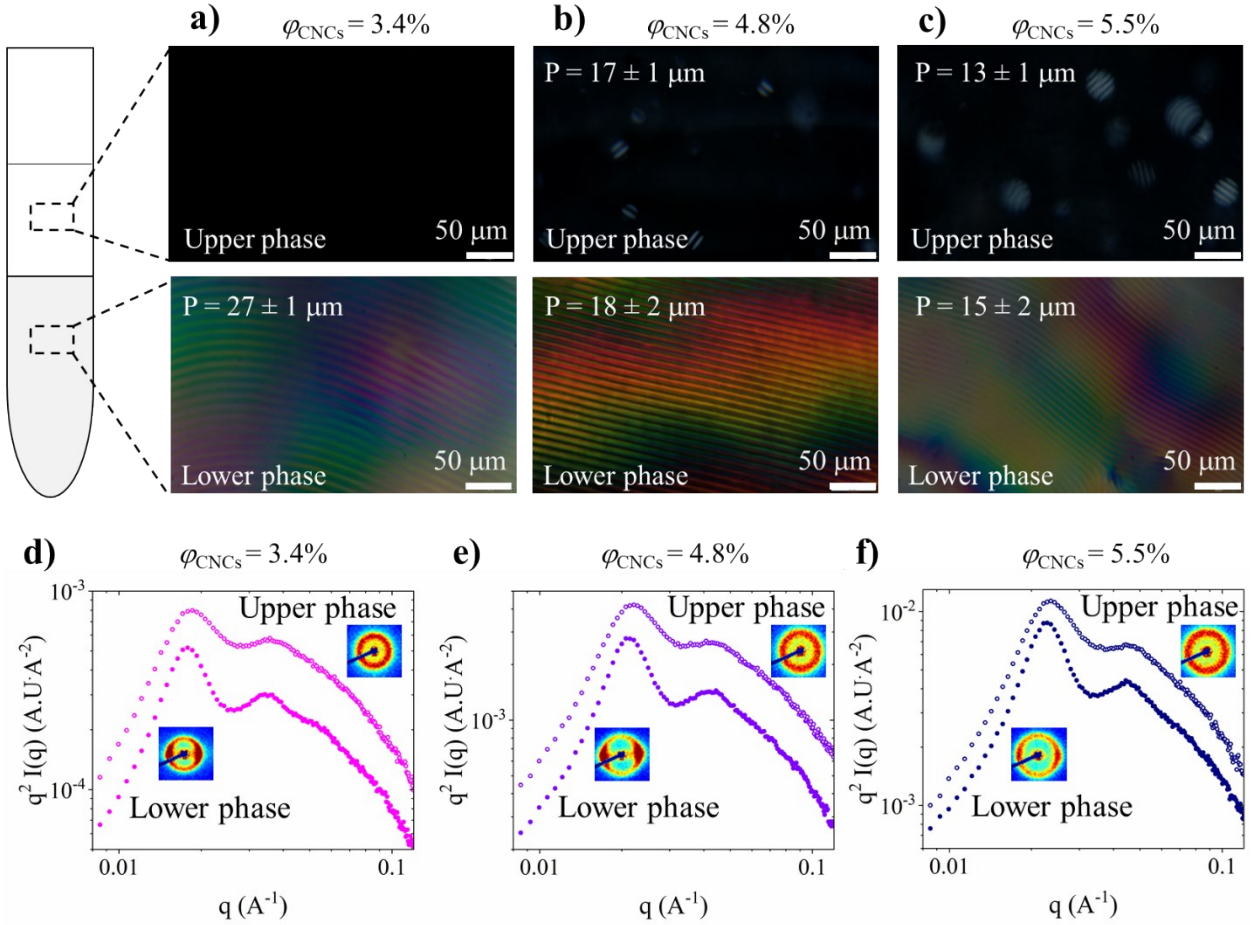

Figure S8. POM images of the upper (macroscopically isotropic) and lower (birefringent) phases of a) 3.4 vol%, b) 4.1 vol%, and c) 5.5 vol% CNCs in water. d)-f) Log-Log Lorentz-corrected intensities ($I \times q^2$) as a function of the scattering vector q of the upper (empty symbols) and lower (filled symbols) phases of 3.4, 4.1, and 5.5 vol% CNCs suspension in water (respectively). The insets are the corresponding 2D SAXS patterns. The curves are shifted for better visualization.

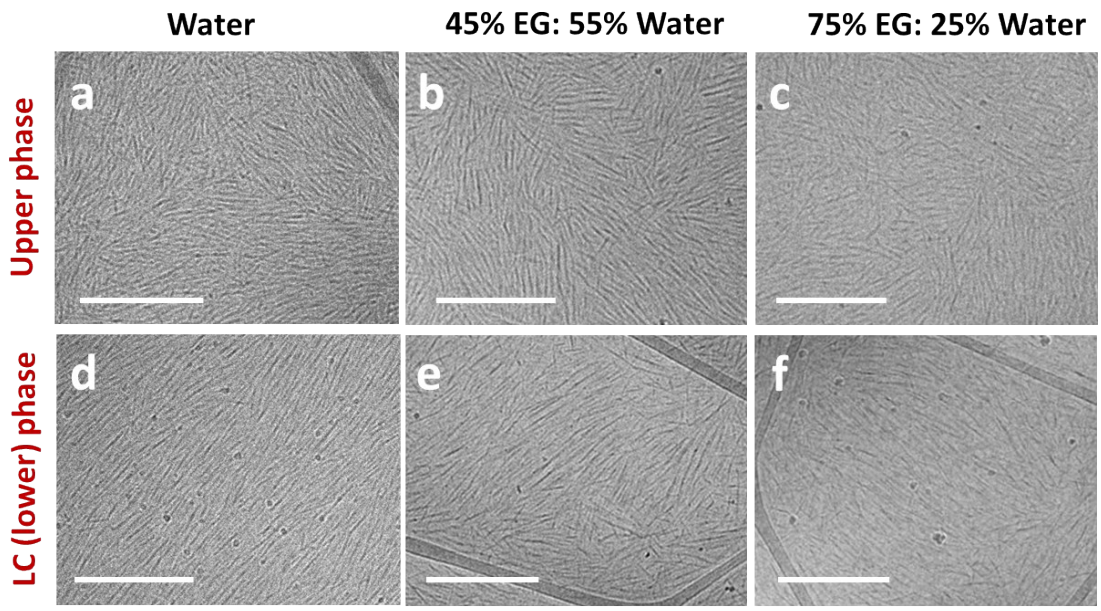

Figure S9. Cryo-TEM images of suspensions of φ_{CNCs} = 4.1%. In water: a) upper and d) lower phase. In liquid mixture of $EG_{45\%}$:$Water_{55\%}$: b) upper and e) lower phase, and in $EG_{75\%}$: $Water_{25\%}$: c) upper phase and f) lower phase. Scale bar = 500 nm.

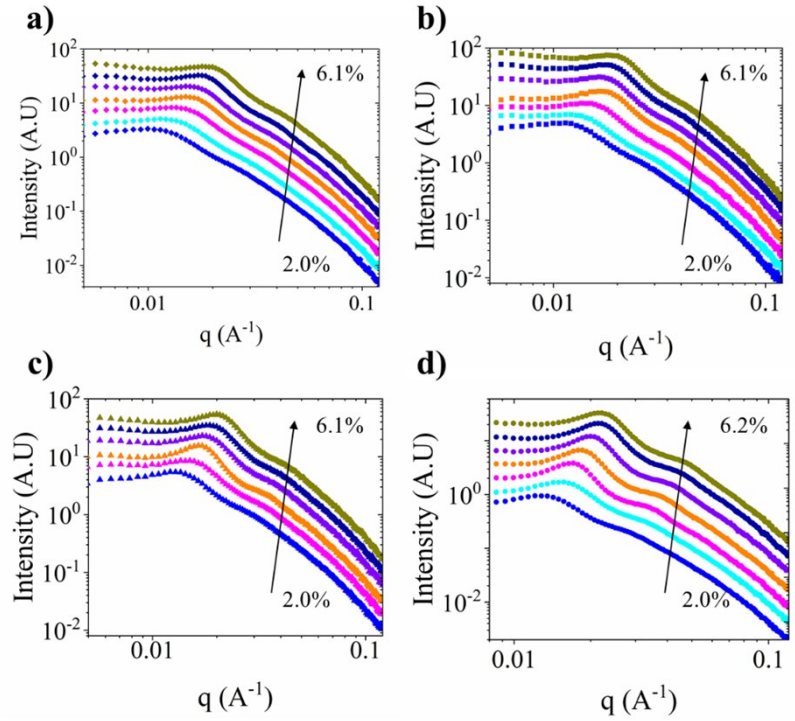

Figure S10. Small-angle scattering curves of CNCs suspensions in a) native EG (◆), b) $EG_{75\%}$:$Water_{25\%}$ (■), c) $EG_{45\%}$:$Water_{55\%}$ (▲), and d) water (●). The color code is identical for all series (φ_{CNCs} = 2.0% ◀, 2.7% ◀, 3.4% ◀, 4.1% ◀, 4.7% and 4.8% ◀, 5.4% and 5.5% ◀,6.1% and 6.2% ◀). The curves are shifted for better visualization.

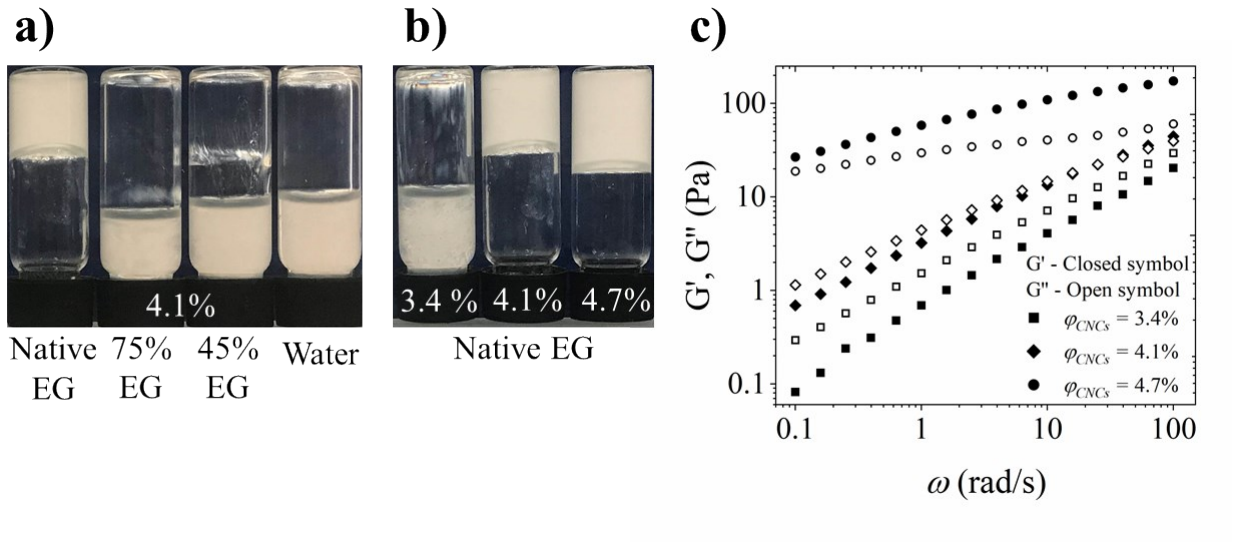

S.8 Flow properties of the suspensions

Figure S11. Images of flipped vials a) 4.1 vol% CNCs in native EG, $EG_{75\%}$:$Water_{25\%}$, $EG_{45\%}$:$Water_{55\%}$, and water (from left to right) and b) 3.4-4.7 vol% CNCs in native EG (from left to right), between two cross polarizers. c) Log-Log plot of the storage modulus G'(closed symbols) and loss modulus G'' (open symbols) as a function of the angular frequency ω of 3.4 vol% (), 4.1 vol% (), and 4.7 vol% () CNCs in native EG.

The viscosity of the suspensions is expected to follow the Krieger-Dougherty equation (exponential growth of the zero viscosity with respect to the concentration of the colloids).[11] Figure S11 a) shows vials containing 4.1 vol% CNCs (φ_{CNCs} = 4.1 %) in the different solvent mixtures turned upside-down. While the suspensions in water, $EG_{45\%}$:$Water_{55\%}$ and $EG_{75\%}$:$Water_{25\%}$ flow and show flow-birefringent, CNCs suspension in native EG do not flow at φ_{CNCs} > 4.1% (Figure S11 b). Oscillatory rheological experiments as a function of the angular frequency for CNCs suspensions in native EG (Figure S10 c) indicate that at φ_{CNCs} < 4.1% the loss modulus G'' takes on higher values than the storage modulus G', showing that up to φ_{CNCs} = 4.1% the suspensions act as viscous liquid. At φ_{CNCs} = 4.7%, the trend is changing and G' takes on higher values than G'', showing that the suspensions act as kinetically arrested glassy phase.

References

1. L. Onsager, *Annals of the New York Academy of Sciences*, 1949, **51**, 627-659.

2. P. J. Flory, *Proceedings of the Royal Society of London. Series A. Mathematical and Physical Sciences*, 1956, **234**, 73-89.

3. P. J. Flory and A. Abe, *Macromolecules*, 1978, **11**, 1119-1122.

4. A. Stroobants, H. N. W. Lekkerkerker and T. Odijk, *Macromolecules*, 1986, **19,** 2232-2238.

5. H. N. W. Lekkerkerker and G. J. Vroege, *Philosophical Transactions of the Royal Society A: Mathematical, Physical and Engineering Sciences*, 2013, **371**, 20120263.

6. J. W. Swan, and E. M. Furst, *Journal of colloid and interface science*, 2012, **388**, 92-94.

7. P. A. Buining, A. P. Philipse and H. N. W. Lekkerkerker, *Langmuir*, 1994, **10**, 2106-2114.

8. Y. Mao, M. Bleuel, Y. Lyu, X. Zhang, D. Henderson, H. Wang and R. M. Briber, *Langmuir*, 2018, **34**, 8042-8051.

9. C. Schütz, M. Agthe, A. B. Fall, K. Gordeyeva, V. Guccini, M. Salajkova, T. S. Plivelic, J. P. Lagerwall, G. Salazar-Alvarez and L. Bergström, *Langmuir*, 2015, **31**, 6507-6513.

10. N. Cohen, G. Ochbaum, Y. Levi-Kalisman, R. Bitton and R. Yerushalmi-Rozen, *ACS Applied Polymer Materials*, 2019.

11. P. Cassagnau, *Polymer*, 2013, **54**, 4762-4775.